Structural characterization of interfaces in epitaxial Fe/MgO/Fe magnetic tunnel junctions by transmission electron microscopy

C. Wang,[1] A. Kohn,[2,*,†] S. G. Wang,[3,4] L. Y. Chang,[1] S.-Y. Choi,[1] A. I. Kirkland,[1] A. K. Petford-Long,[5] and R. C. C. Ward[3,*,‡]

[1]*Department of Materials, University of Oxford, Oxford OX1 3PH, United Kingdom*

[2]*Department of Materials Engineering, Ilse Katz Institute for Nanoscale Science and Technology, Ben-Gurion University of the Negev, Beer-Sheva 84105, Israel*

[3]*Clarendon Laboratory, Department of Physics, University of Oxford, Oxford OX1 3PU, United Kingdom*

[4]*State Key Laboratory of Magnetism, Beijing National Laboratory for Condensed Matter Physics, Institute of Physics, Chinese Academy of Sciences, Beijing 100190, China*

[5]*Center for Nanoscale Materials, Argonne National Laboratory, 9700 South Cass Avenue, Lemont, Illinois 60439, USA*

(Received 4 May 2010; revised manuscript received 23 June 2010; published 28 July 2010)

We present a detailed structural characterization of the interfaces in Fe/MgO/Fe layers grown by molecular-beam epitaxy using aberration-corrected transmission electron microscopy (TEM), scanning TEM, and electron energy-loss spectroscopy. When fabricated into magnetic tunnel junctions, these epitaxial devices exhibit large tunnel magnetoresistance ratios (e.g., 318% at 10 K), though still considerably lower than the values predicted theoretically. The reason for this discrepancy is being debated and has been attributed to the structure of, and defects at the interface, namely, the relative position of the atoms, interface oxidation, strain, and structural asymmetry of the interfaces. In this structural study, we observed that Fe is bound to O at the interfaces. The interfaces are semicoherent and mostly sharp with a minor degree of oxidation. A comparison of the two interfaces shows that the top MgO/Fe interface is rougher.

DOI: 10.1103/PhysRevB.82.024428 PACS number(s): 87.64.Ee, 75.70.Cn, 72.25.−b

I. INTRODUCTION

Following theoretical predictions[1,2] of tunneling magnetoresistance (TMR) in epitaxial Fe/MgO/Fe junctions, TMR ratios of approximately 200% were measured at room temperature for CoFe/MgO/CoFe and fully epitaxially Fe/MgO/Fe junctions.[3–8] Significant progress has been since achieved with sputter-deposited CoFeB/MgO/CoFeB magnetic tunnel junctions (MTJs) in which the CoFeB ferromagnetic electrode is amorphous.[9–11] For these MTJ, TMR ratios of 604% at room temperature have been reported,[9] which is of interest for technological applications such as in magnetic random access memory and magnetic sensors. However, these values, and especially the TMR ratio of the model epitaxial Fe/MgO/Fe MTJ are still considerably lower than the predictions based on first-principles calculations.[1,2] Consequently, revealing the physical origin of this discrepancy may further contribute to understanding the large TMR ratio in MgO-based MTJ, as well as associated experimental observations such as asymmetric bias voltage dependence.[4]

Calculations[12] have shown that the TMR value is significantly reduced if the interfaces are oxidized though recent experimental work shows that the effect of oxidation may not be as significant as expected by those calculations[13] but rather the degree of strain.[14] The asymmetry and decrease in the TMR ratio have been attributed to interface phenomena: dislocations,[15] electronic structure of the Fe/MgO interface,[5] and the formation of an Fe-O layer.[12,16,17] Therefore, to better understand their role on electron tunneling, these interfaces have been characterized by surface x-ray diffraction, Auger electron spectroscopy, x-ray absorption spectra, x-ray magnetic circular dichroism, x-ray photoelectron spectroscopy, spin-dependent tunneling spectroscopy, and transmission electron microscopy (TEM).[12–20]

In this work, we report on a detailed structural characterization of epitaxial Fe/MgO/Fe layers, which when fabricated to a MTJ, achieved a TMR value of 170% at room temperature.[6,16] Although fully epitaxial structures will probably not be used in commercial devices, they are model systems to compare experimental results and theoretical calculations and to study spin-polarized coherent tunneling.[4–7]

In particular, the aim of this work is to characterize the interface structure of epitaxial Fe/MgO/Fe multilayers, which when fabricated into MTJ devices, demonstrate among the highest TMR ratios to date. To achieve this aim, we use aberration-corrected TEM and scanning TEM (STEM).

Revealing the atomic structure of the Fe/MgO interface is important because this information is the basis for theoretical calculations.[1,2] Experimental characterization of the interfacial structure that has been used as input for such calculations was undertaken by *in situ* measurements. Urano and Kanaji[20] reported that Fe atoms are adjacent to O ions at the Fe/MgO (001) interface after the first monolayer growth, as measured by low-energy electron diffraction. However, such *in situ* characterization during growth does not account for structural alteration that may occur after completing the fabrication of the device, for example, due to strain relaxation. Therefore, an *ex situ* measurement such as TEM, can be advantageous in characterizing the atomic structure of the actual device. Here, we have investigated the atomic structure across the interface, namely, how the Fe atomic columns are positioned with respect to the Mg or O columns. This was studied by recording high angle annular dark field (HAADF)-STEM images in which the contrast is related to the atomic number.[21] As the atomic number of Fe is considerably larger than that of Mg or O, a HAADF-STEM image

allows us to identify the relative positions of the atomic columns.

As described earlier, the structure of the Fe/MgO interfaces, for example, whether the terminating Fe layer is oxidized, is predicted to influence significantly the TMR ratios.[12,22,23] Various *in situ* techniques including surface x-ray diffraction[24] and x-ray magnetic circular dichroism[25,26] have been used to characterize the Fe/MgO interface structure, arriving at conflicting conclusions. Serin *et al.*[18] measured an asymmetry in the roughness of the two interfaces, using STEM to collect electron energy-loss spectroscopy (EELS) data. However, the data were collected along the MgO [001] direction, namely, along atomic columns that combine Mg and O atoms. In this work, we examine the samples along the Mg [011] direction, in order to differentiate between O and Mg atomic columns. In addition, the thickness of the MgO barrier in our samples is 3 nm, which is applicable for MTJ devices.

We characterized the oxidation structure at the interface, by comparing experimental high-resolution aberration-corrected TEM images with simulated ones, and also measuring the interplanar distances between Fe and MgO layers. We conclude that for the growth conditions used in this research for the fabrication of MTJ structures, the interfaces are predominately sharp, though we cannot rule out the possibility of a minor component of oxidation at the interfaces.

Finally, the growth modes of the Fe/MgO/Fe junction, namely, MgO growth on Fe followed by Fe growth on MgO, are important in determining the spin-dependent transport properties. The structure of the two interfaces has been compared by *Z*-contrast HAADF-STEM images and EELS. This study shows that the top Fe/MgO interface is rougher than the bottom one.

II. EXPERIMENTAL DETAILS

Epitaxial multilayers with the following structure Fe(50)/MgO(3)/Fe(10) structures (thickness of layers in nanometer) were deposited on MgO (001) single-crystal substrates. The epitaxial relation of the layers, Fe(001)[100]/MgO(001)[110]/Fe(001)[100], is well characterized. Detailed growth information and structural characterization using reflection high-energy diffraction, and x-ray diffraction are presented elsewhere.[6,16,19,27]

The samples were prepared by molecular-beam epitaxial growth on MgO (001) single crystals at a base pressure of 5×10^{-11} mbar. Prior to the growth, the MgO substrates were degreased by boiling successively in trichloroethylene, propan-2-ol and methanol and then annealed at 500 °C for 30 min in ultrahigh vacuum. A 10-nm-thick MgO buffer layer was grown to prevent carbon contamination. Then, the bottom Fe layer was deposited at 200 °C and annealed at 400 °C. The MgO barrier was deposited at room temperature followed by the top Fe electrode at 200 °C. Finally, a Cr capping layer was deposited to prevent oxidization. Depositions of both MgO and Fe are achieved by e-beam evaporation of single-crystal MgO and high-purity Fe materials. The growth rates of Fe and MgO were 0.03 nm/s and 0.01 nm/s, respectively.

During growth of the MgO layer, an increase in the partial pressure at mass 32 from below detection levels to around 2.5×10^{-12} mbar was measured. Similar observations were reported by Yuasa *et al.*,[4] suggesting that the residual gas is oxygen due to the decomposition of the MgO source. This phenomenon may result in oxygen vacancies in the MgO barriers, which will be further discussed in this report.

A JEOL-2200FS TEM equipped with two aberration correctors[29] was used to acquire both high-resolution TEM (HRTEM) and HAADF-STEM images of the Fe/MgO interfaces. In TEM mode, a negative C_3 (third-order spherical aberration), measured at -6 ± 5 μm, combined with the defocus value was used to compensate for C_5 (so-called "C_5 balanced condition"[30]). For HAADF-STEM imaging, the inner- and outer-collection semiangles were 50 mrad and 140 mrad, respectively. The spatial resolution in STEM mode is approximately 0.1 nm.

In order to study possible oxidization at the bottom Fe/MgO interface, the two reported models of sharp[1] and oxidized[24] interfaces were used for the TEM image simulation. We note that the TEM cross-sectional specimens were cut along the MgO [110] direction so that Mg and O atomic columns can be observed individually. Detailed information on TEM sample preparation and multislice image simulation methodologies can be found in our previous paper.[31] The entire focal series was compared to image simulations in order to confirm the structure and thickness of the sample. Here, we show a single image from these series, typically at Gaussian focus.

The EEL spectra for these samples were acquired at the "SuperSTEM" facility,[32] using a modified VG501 STEM with a cold field-emission gun, equipped with a Nion second generation spherical aberration corrector[33] and a Gatan Enfina electron energy-loss spectrometer. The convergence angle of the electron probe was set at 24 mrad for both imaging and spectroscopy modes. The collection angle for EEL spectra was 19 mrad. The inner and outer angle for the HAADF imaging was 70 mrad and 210 mrad, respectively. The energy resolution is 0.6 eV, which is determined by the chosen energy dispersion of the spectrometer at 0.3 eV, respectively.

The relative Fe and O atomic concentrations were calculated according to the following steps, using a script written by Gatan for DIGITALMICROGRAPH 3.10. After removing the background signal using a power-law relation, the relative composition or atomic areal density of O and Fe were compared using the hydrogenic (white lines) model[34] at each point. In order to improve the signal-to-noise ratio, multivariate statistical analysis[28,35,36] was employed.

III. RESULTS AND DISCUSSION

Figure 1 shows an overview of the multilayer structure using a low magnification HAADF-STEM image. Areas in the image showing larger intensity (brighter contrast) correspond to the Fe layers due to the higher atomic number of Fe relative to MgO while the MgO regions have lower intensity.

We first characterize the structure at the interface region between the MgO substrate and the bottom Fe layer using

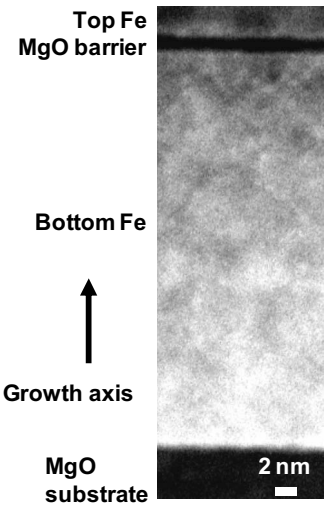

FIG. 1. HAADF-STEM image showing an overview of the MTJ multilayer structure.

HAADF STEM. Due to the crystallographic quality of the substrate and the flatness of this interface, we can determine the relative positions of the atomic columns. This analysis also allows for a more reliable characterization of the Fe/MgO interface in the MTJ structure itself.

A. Structure of the interface between the bottom Fe electrode and MgO substrate

An atomic resolution HAADF-STEM image of the MgO substrate/bottom Fe interface along the MgO [110] zone axis is presented in Fig. 2. The atomic columns with the brighter contrast correspond to the Fe columns, whereas those with lower contrast correspond to the Mg columns. However, O atomic columns are not clearly visible because of its low atomic number. Two types of rows are marked in Fig. 2(a), referred to as A and B, repeated along the in-plane MgO [001] direction. The atomic structure of rows A and B, assuming a sharp interface, is shown schematically in the inset based on the intensity from the Fe and Mg atomic columns in the experimental image. The difference between the rows is that for A, Fe atoms are positioned directly adjacent to O atoms at the interface, whereas for B, Fe atoms are separated by one atomic plane from the Mg columns at the interface. This atomic configuration fits the model shown in the inset of Fig. 2(a) showing that the Fe columns are positioned adjacent to the O columns at the interface.

In order to confirm this atomic arrangement, two line scans of the image intensity were performed along columns without background subtraction as shown in Fig. 2(b). An intensity line scan of a type A column shows that the peak to background intensity value of the Fe HAADF signal is approximately twice as large than for the Mg signal (the atomic column associated with the HAADF signal is denoted schematically by circles in the figure). Arrow C denotes schematically the location at which the oxygen column would be expected for a sharp interface. However, from these results, we cannot detect an oxygen column because the HAADF intensity at point C is close to the background level of the

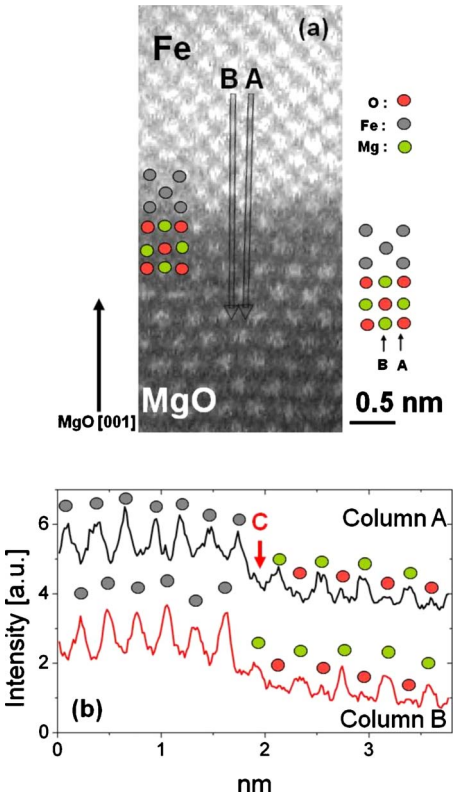

FIG. 2. (Color online) (a) High-resolution STEM image of the interface between the bottom Fe and MgO substrate, obtained along the MgO [110] direction; (b) two line scans of the intensity of the HAADF signal obtained from atomic columns along the directions denoted schematically by arrows A and B. Inset: the atomic arrangement of the Fe and MgO layers.

measurement. Away from the interface, the positions of oxygen atomic columns are detected more clearly.

For the column B line scan, Fe atomic columns are positioned above the Mg columns. The atomic arrangement away from the interface shows that positions of Fe, Mg, and O columns are complimentary to those observed in column A. In this case, we note that the intensities of the Mg atomic columns adjacent to the interface are lower, which may be attributed to misalignment of the electron probe or variations in sample thickness.

Both of these intensity scans confirms that the arrangement agrees with the model drawn in the inset. Although the detection of oxygen columns at the interface is not conclusive from these data (see following section), these HAADF-STEM measurements characterize the alignment of Fe, Mg, and O atomic columns between the bottom Fe electrode and the MgO substrate. These experimental results are in agreement with *in situ* measurements[20] and the atomic arrangement used for theoretical calculations.[1,37] In the following section, we focus on the structure of the interface between the bottom Fe electrode and the MgO tunneling barrier.

B. Structure of the interface between the Fe electrode and MgO barrier

Figure 3 presents an HRTEM image overview of the MTJ structure obtained along the [100] zone axis of MgO, in this

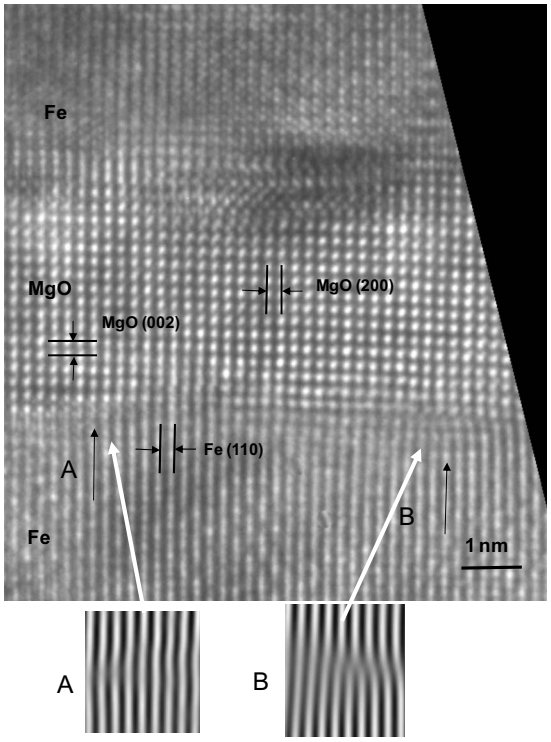

FIG. 3. A HRTEM image from the bottom Fe electrode and MgO barrier. The zone axis is MgO [100]. The interface in region A is coherent while a dislocation is observed in region B. The two insets are images reconstructed from the reflections of MgO (100) and Fe (110) in power spectra calculated from regions A and B, respectively.

case using a conventional TEM (JEOL 3000F). The epitaxial quality of MgO is evident as both (002) planes and (200) planes are observed throughout the entire barrier. The lattice spacing of the Fe (002) planes is not resolved due to the resolution limit of this microscope. Inset A, which shows an image that was reconstructed from a power spectrum using the MgO (100) and Fe (110) reflections, demonstrates a region of a coherent interface between the Fe and MgO epitaxial layer. In the case of inset B, a similar image reconstruction highlights a dislocation, which originates from the approximately 3.5% lattice mismatch between the MgO (100) and Fe (110) planes. This result shows that the interface is semicoherent, namely, the first aspect we observe at these Fe/MgO interfaces that deviates from the ideal description. Such defects may contribute to a reduction in the experimental TMR values when compared to those predicted theoretically for ideal coherent interfaces. Bonell *et al.*[14] reported that a reduction in the lattice mismatch between the MgO barrier and the ferromagnetic electrode, using an Fe-V alloy, results in an increase in the TMR ratio.

Several experimental techniques have been applied to study the structure of the Fe/MgO interface, in particular, to determine the existence of an Fe-O monolayer. Meyerheim *et al.*[17,24] used *in situ* surface x-ray diffraction during MgO e-beam deposition on a single crystalline Fe (001) substrate, concluding that an FeO layer is indeed formed at the interface. Yu's density-functional theory calculations[37] of such an interface resulted in an Fe-O interlayer distance of 0.247 nm, which is in reasonable agreement with Meyerheim's result. However Sicot *et al.*[38] and Miyokawa *et al.*[25] characterized the Fe/MgO interface *in situ* using x-ray absorption spectroscopy and x-ray magnetic circular dichroism, respectively, from which they concluded that the interface is sharp, i.e., there is no Fe-O monolayer. Oh *et al.*[39] suggested that the interface is partially oxidized based on high-resolution electron EELS. Again, we note that these experiments were based on *in situ* measurements, which may not reflect the final structure of the MTJ.

Recently, Serin *et al.*,[18] applied EELS at the atomic scale to study MTJ multilayers using STEM, namely, *ex situ*, with the electron beam aligned along the MgO [100] direction. They reported that Fe and MgO terraces can overlap, extending parallel to the interface over typical widths of 6–10 nm and heights below 1 nm. In addition, for a 10-nm-thick MgO barrier, a structural asymmetry was reported in which the top interface was found to be rougher.

Our previous work[31] focused on characterizing the Fe/MgO interface using conventional HRTEM. That study indicated that the interfaces are sharp, though due to aberrations of the microscope, oxygen atomic columns could not be imaged directly. Consequently, the differences between experimental and simulated HRTEM images of sharp and oxidized interfaces are subtle. In order to differentiate clearly between the oxidized and nonoxidized interfacial models, we apply here aberration-corrected HRTEM to image oxygen atomic columns at the interface. Several studies have proved that it is indeed practical to image oxygen columns using aberration-corrected microscopy.[40,41]

Figure 4(a) presents a comparison between an experimental HRTEM image (center) with simulated images (left and right). The simulated images of oxidized and sharp interfaces are shown on the left and right sides of the experimental image in Fig. 4(a), respectively. The structures used for simulating these HRTEM images are shown in Figs. 5(a) and 5(b) for the oxidized and sharp interfaces, respectively. The experimental image shown in this figure was recorded near the C_5 balanced condition[30] and at the Gaussian focus. The best fit between the experimental and simulated focal series images is for a sample thickness of 6 nm.

For aberration-corrected HRTEM images, the difference between the two proposed models is significant and can be observed directly in the simulated images. In the oxidized model, oxygen columns are observed (marked by the arrow in the simulated image) in the first Fe layer, whereas this feature does not appear in the case of the sharp Fe/MgO interface.

We note that sharp interfaces, which include atomic steps, could potentially be also interpreted as oxidized interfaces because the HRTEM image is a two-dimensional projection of the sample. However, image simulations of sharp interfaces in which atomic steps were introduced resulted in significantly different contrast compared with oxidized interfaces.[42] This observation is in agreement with the report of Serin *et al.*,[18] regarding typical terrace widths of 6–10 nm, which is comparable to our sample thickness.

A line scan measuring the image intensity was applied to the first MgO atomic layer along the in-plane MgO [100] direction. The aim of this measurement is to confirm the

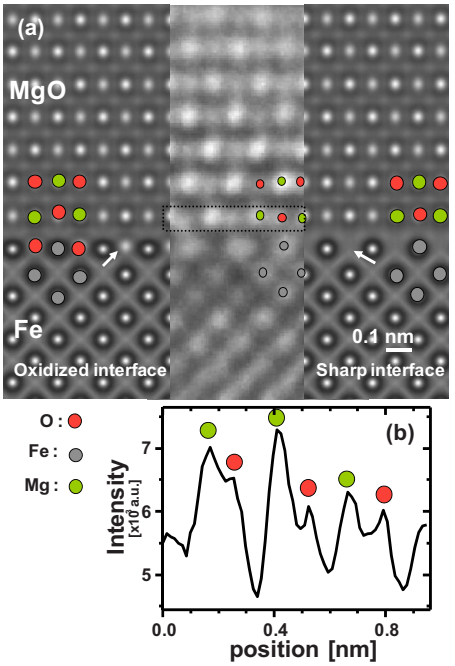

FIG. 4. (Color online) (a, center) A HRTEM image from a focal series recorded at near C_5 (fifth-order aberration) balanced conditions, Gaussian defocus, compared with simulated images of 6-nm-thick samples: (a, right) sharp interface and (a, left) oxidized interface. The inset shows the atomic arrangement at the interface. (b) An intensity scan along the first MgO layer above the bottom Fe electrode over a width of 0.1 nm from the region denoted by a box in (a).

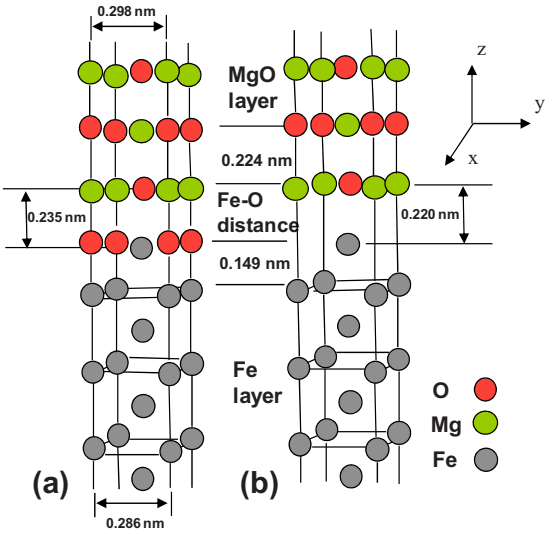

FIG. 5. (Color online) Structural input for HRTEM multislice image simulations in the case of (a) an oxidized interface with an FeO layer at the Fe and MgO interface; and (b) a sharp Fe/MgO interface. The interplanar distance at the interface is 0.235 nm for the oxidized model (Ref. 24) and 0.220 nm for the sharp interface (Ref. 31).

detection of oxygen atomic columns, shown in Fig. 4(b). The intensity scan highlights the position of the Mg and O atomic columns in the tunnel barrier, demonstrating that the imaging condition used in this work enables identification of these low atomic number atoms. However, no oxygen columns were observed in the first Fe layer, indicating that in this region, the interface is sharp. Through the comparison with the simulated models, the interplanar distance of Fe-O is measured to be 0.220 ± 0.005 nm, which agrees well with the result from our previous conventional TEM analysis.[31] Measurement statistics are limited when analyzing cross-sectional TEM images. However, similar analysis of several interface regions concluded that the interface is sharp.

In order to remove residual aberrations and further improve the signal-to-noise ratio of the images, the phase of the exit electron wave was reconstructed using a focal series of aberration-corrected HRTEM images. Figure 6(a) presents the phase of the electron wave at the exit plane of the sample. The phase was reconstructed from a series of 20 images acquired with defocus values ranging from −40 to +40 nm at a focal step of 4 nm. For the case of thin specimens, which can be considered as weak phase objects, the bright contrast in the reconstructed phase can be directly correlated with the atomic column sites.[43]

A line scan of the electron phase values inside the MgO barrier along the in-plane MgO $[\bar{1}10]$ direction is shown in Fig. 6(b), which shows both O and Mg atomic columns. The measured intensity of the oxygen column is less than the Mg columns since its projected potential is weaker. Variations in the peak intensities attributed to the same type of atomic column can be due to surface contamination and damage, and small thickness variations. Another scan was performed along the first Fe layer in order to examine whether it is oxidized. As illustrated in Fig. 6(c), in most cases intensity peaks associated with Fe atomic columns are clearly separated, though a small peak is observed between two such intensity maxima. This observation may be attributed to the presence of oxygen showing that a minor part of the interface may be oxidized. Additionally, this result may also be explained by a tilt of the crystal specimen away from the zone axis. This tilt can be observed particularly in Fe layers (Fig. 6), as streaked elongated features along the Fe [110] diagonal direction.

Another intensity scan along the [001] growth direction is shown in Fig. 6(d). A signal from an oxygen column is detected directly adjacent to the Fe columns, in agreement with our previous HAADF-STEM observation and consistent with theoretical predictions,[20] namely, that Fe bonds with the O at the interface. With respect to atomic steps at the interface, the reconstructed phase cannot determine conclusively the existence of these because this methodology is not sensitive enough to the small effective variations in atomic number. However, as described previously, HRTEM image simulations of atomic steps at the interface were significantly different from the experimental data and the proposed model for the oxidized interface.

In summary of this section, the interface between the MgO barrier and bottom Fe electrode is predominately sharp. The existence of a sharp interface can explain the high TMR values [170% at room temperature and 318% at 10 K (Ref. 6)] achieved in devices based on this growth protocol. Conversely, the detection in our samples of dislocations and possible minor oxidization at the interface may explain why the

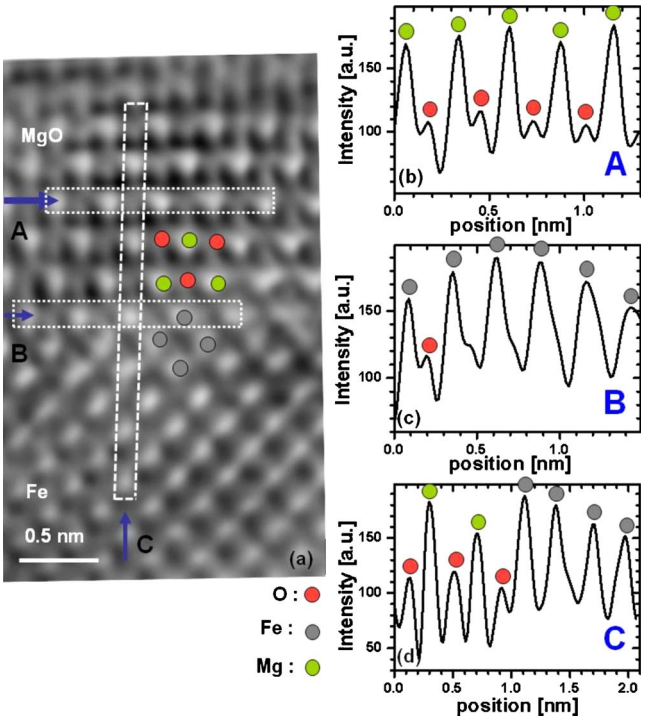

FIG. 6. (Color online) (a) Reconstructed phase of the exit wave function from a through-focal series of HRTEM images in the JEOL 2200FS with Cs at −5 μm. (b) An intensity scan across the MgO barrier region denoted by arrow A, (c) an in-plane intensity scan from the first Fe layer denoted by arrow B, and (d) an intensity scan along the growth direction denoted by arrow C. The width of the line scan is 0.08 nm. The zone axis is MgO [110]. Note: the term intensity refers to the reconstructed phase.

TMR values are lower than the theoretical predictions based on an ideal interface model.

C. Growth modes of the electrode and barrier

A HAADF-STEM image of both Fe electrodes and the MgO barrier is shown in Fig. 7. The bottom interface appears smooth while the top interface has considerably more atomic column steps, typically one or two atomic planes in width, marked by arrows in Fig. 7. This observation agrees with a previous report[44] and is further studied in this section using EELS measurements.

A typical HAADF image of the barrier region, obtained using the SuperSTEM instrument, is shown in Fig. 8(a). The top Fe electrode is seen in the left part of the image and the bottom Fe electrode is on the right side. An EELS line scan acquired with spatial steps of 0.16 nm was recorded along the direction shown schematically by the rectangle denoted in the image, starting from the top electrode.

The atomic ratio between Fe and O is plotted as a function of spatial position in Fig. 8(b). The relative error of the composition content is estimated at ~10%. From the start of the composition profile in the top electrode, the Fe content is high though an oxygen content of approximately 10 at. % is measured, attributed to surface oxidization of the TEM sample. Near the top interface, the Fe composition decreases

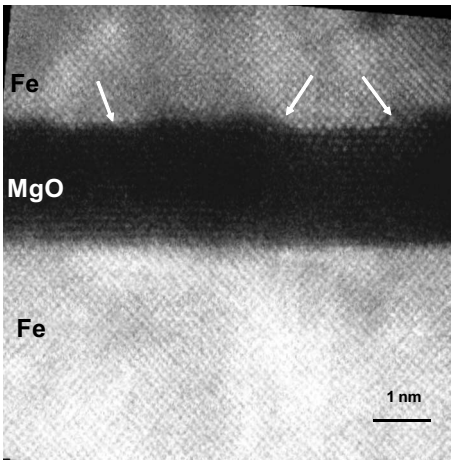

FIG. 7. *Z*-contrast HAADF-STEM image from the MgO barrier. (The position of steps at the top interface are denoted by arrows.) The zone axis is MgO [110].

while the oxygen content increases with the transition into the MgO barrier and possible intermixing of Fe and O due to roughness observed at that interface. Inside the barrier, the Fe signal is still visible in the spectra resulting in an apparent Fe concentration of less than 10%. The inset of Fig. 8 is one such EEL spectrum measured at the center of the tunneling

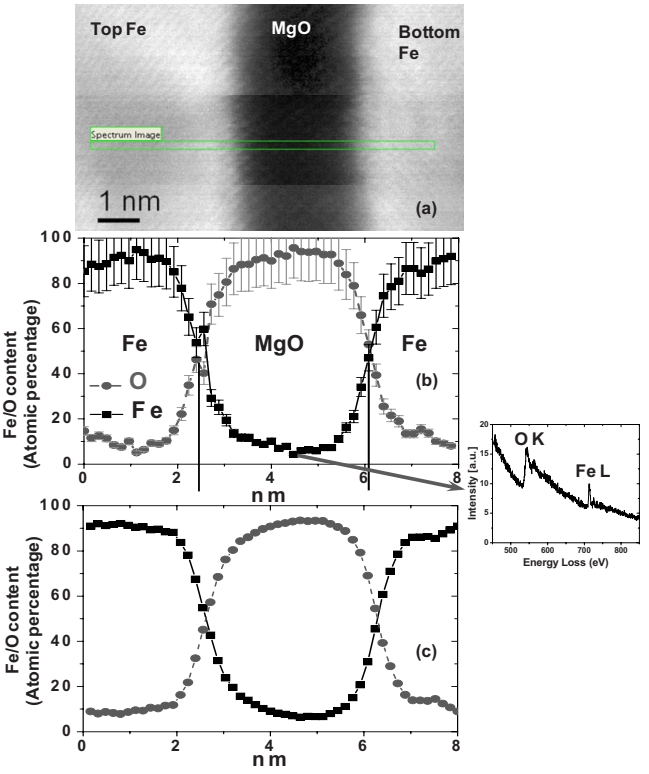

FIG. 8. (Color online) (a) *Z*-contrast STEM image from the barrier region; (b) the atomic ratio of O and Fe across the MgO and Fe layers derived from EEL spectra measured along the direction denoted schematically by the rectangle shown in (a). The inset is a spectrum from the middle of the MgO barrier apparently showing a large Fe content (c) the composition profiles for O and Fe derived from the EEL spectra data of (b) and applying MSA.

barrier, which shows clearly the Fe *L* edge. In the following paragraph, we attribute this result to an artifact due to geometric broadening of the electron probe. Toward the bottom electrode, the Fe signal increases eventually reaching nearly 90%. Qualitatively, it can be observed in Fig. 8(b) that the relative change in Fe/O composition at the two interfaces is different, namely, the bottom interface appears sharper than that of the top interface.

In order to further analyze this observation, Fig. 8(c) shows the same composition profiles for O and Fe deduced from EELS data, after reconstruction using multivariate statistical analysis with two sets of eigenvalues.[28,36] This analysis results in a reduction in the signal noise compared with the composition profiles calculated from the raw data in Fig. 8(b). Here too, we observe that the change in Fe and O concentration across the top interface appears more gradual than that across the bottom interface. As the composition profile can be fitted to an error function, the width of the interface can be defined as the distance between fractions of 0.84 and 0.16 of the maximum Fe or O content. The widths of the top and bottom interfaces are estimated to be 1.3 nm and 1 nm, respectively. Similar analysis on a sample with a thinner bottom Fe electrode resulted in a similar conclusion regarding the asymmetry of the interfaces.

In order to examine whether this result, and the detection of Fe in the MgO barrier are measurement artifacts due to broadening of the electron probe[45] resulting from the sample thickness, we applied a geometrical model described in Refs. 46 and 47. This approach enables to estimate the volume in the sample from which the signal is acquired during these measurements. The sample thickness was estimated by the ratio of the zero loss to plasmon peaks, and the geometry of the electron beam is defined by the convergence semiangle. We note that the top interface is closer to the hole of the TEM sample, namely, a thinner region. Qualitatively, if we assume that the two interfaces are identical, geometrical broadening of the electron beam at the top interface would be reduced, thus appearing to result in a smoother interface. However, the measurements show that the top interface is in fact rougher. In addition, calculations of the geometric beam broadening for these experimental conditions[42] explain the apparent detection of Fe at the center of the MgO barrier. Here, the diffusion of Fe into the epitaxial MgO barrier appears as mostly a measurement artifact of the EELS analysis. Such significant diffusion is not expected due to the relatively low growth temperature.

This asymmetry in the two interfaces, attributed to roughness or intermixing, may be a result of different growth mechanisms or growth protocol. Seabourne *et al.* examined the O *K* edge energy-loss near-edge structure of EEL spectra obtained from this sample. Using the *ab initio* density-functional theory code CASTEP, a better fit to calculations was found for a sharp interface rather than an oxidized interface.[48]

Fe growth on MgO is a three-dimensional island mode.[49] However, in the case of the bottom electrode, the Fe layer is thick (50 or 100 nm) and undergoes thermal annealing, which results in an epitaxial and smooth layer.

On this surface, we can expect the MgO to wet the underlying Fe layer due to the relatively low surface energy of MgO [calculated at 1.16 J/m^2 for the (001) plane][50] compared to that of Fe [calculated at 2.94 J/m^2 and approximately 2.2 J/m^2 for a polycrystalline material at 298 K and Fe (001) plane, respectively].[51,52]

Therefore, the bottom barrier interface is smooth compared to the top barrier interface. The relatively large lattice mismatch (~3.5%), and consequently low critical thickness (~1 nm) (Ref. 44), as well as the low growth temperature of MgO, may tend to roughen the top MgO barrier/Fe interface as observed experimentally.

IV. SUMMARY

The aim of this electron microscopy study was to characterize the interface structure in an epitaxial Fe/MgO/Fe multilayer used for the fabrication of MTJ. Such a detailed study can clarify the differences between the input structures used for theoretical calculations of spin-dependent tunneling and the actual structure of an epitaxial MTJ device. These differences may then explain the discrepancies between calculated and experimentally measured TMR ratios. First, we verified the atomic structure at the Fe/MgO interface, namely, how the Fe atomic columns are positioned with respect to the Mg or O columns, using atomic resolution *Z*-contrast HAADF Cs-corrected STEM. The results show that Fe columns are positioned on top of the O columns, in agreement with previous *in situ* measurements by low-energy electron diffraction.[20]

Using aberration-corrected TEM,[29] experimental and simulated Cs-corrected HRTEM images distinguish directly between models of sharp[1] and oxidized[24] interfaces by enabling to image oxygen atomic columns along the MgO [011] direction. HRTEM imaging of the bottom MgO/Fe interface suggests that the interface is predominately sharp. The measured interplanar distance of Fe-O, 0.220 ± 0.005 nm, at the MgO/Fe interface agrees with theoretical calculations of a sharp interface.[37] Reconstruction of the phase of the exit electron wave[43] verified again that the interface is sharp. We note the possibility that a minor fraction of the interface may be oxidized though we cannot differentiate this result from measurement artifacts.

Calculations show that oxygen vacancies can cause a substantial reduction in TMR.[53] Experimentally, Bonell *et al.*[13] fabricated MTJ with controlled addition of oxygen at the interface. A relatively small reduction in the TMR ratio was reported with increasing interface oxidation. Further calculations of Fe/MgO/Fe MTJ are required in order to quantify the relative significance of dislocation defects and minor oxidation, which were both observed in our samples.

Z-contrast STEM images and a compositional analysis using Fe *L* and O *K* edges in EEL spectra show that the top MgO/Fe interface in the MTJ is rougher than the bottom one. This asymmetry of interface roughness may be attributed to lattice mismatch and low critical thickness for strain relaxation of the MgO layers. Note that the relative low surface energy of MgO compared to that of Fe suggests in fact a reduction in roughness of the top interface. This observation may be due to the large difference in growth temperatures of the bottom Fe electrode and MgO barrier. Therefore, the

structure of interfaces in epitaxial MTJ appears significantly different from an ideal equilibrium model used in theoretical calculations, which assumes that both interfaces are sharp and smooth.

ACKNOWLEDGMENTS

We are grateful to Keith Belcher for technical support and to the Engineering and Physical Sciences Research Council (EPSRC) for funding this research project. A.K. thanks the Royal Academy of Engineering and the U.K. Engineering and Physical Sciences Research Council. S.G.W. thanks the National Basic Research Program of China under Grant No. 2009CB929203 and the National Natural Science Foundation of China under Grant No. 50972163 for financial support. A.K.P.L. is funded by Argonne National Laboratory, supported by the U.S. Department of Energy, Basic Energy Sciences, under Contract No. DE-AC02-06CH11357.

*Corresponding author.
†akohn@bgu.ac.il
‡roger.ward@physics.ox.ac.uk

[1] W. H. Butler, X.-G. Zhang, T. C. Schulthess, and J. M. MacLaren, Phys. Rev. B **63**, 054416 (2001).
[2] J. Mathon and A. Umerski, Phys. Rev. B **63**, 220403(R) (2001).
[3] S. S. P. Parkin, C. Kaiser, A. Panchula, P. M. Rice, B. Hughes, M. Samant, and S. H. Yang, Nature Mater. **3**, 862 (2004).
[4] S. Yuasa, T. Nagahama, A. Fukushima, Y. Suzuki, and K. Ando, Nature Mater. **3**, 868 (2004).
[5] C. Tiusan, J. Faure-Vincent, C. Bellouard, M. Hehn, E. Jouguelet, and A. Schuhl, Phys. Rev. Lett. **93**, 106602 (2004); R. Guerrero, D. Herranz, F. G. Aliev, F. Greullet, C. Tiusan, M. Hehn, and F. Montaigne, Appl. Phys. Lett. **91**, 132504 (2007).
[6] S. G. Wang, R. C. C. Ward, G. X. Du, X. F. Han, C. Wang, and A. Kohn, Phys. Rev. B **78**, 180411(R) (2008).
[7] S. Yuasa, A. Fukushima, H. Kubota, Y. Suzuki, and K. Ando, Appl. Phys. Lett. **89**, 042505 (2006).
[8] S. G. Wang, R. C. C. Ward, G. X. Du, X. F. Han, C. Wang, and A. Kohn, IEEE Trans. Magn. **44**, 2562 (2008).
[9] G. X. Miao, K. B. Chetry, A. Gupta, W. H. Butler, K. Tsunekawa, D. Djayaprawira, and G. Xiao, J. Appl. Phys. **99**, 08T305 (2006).
[10] Y. M. Lee, J. Hayakawa, S. Ikeda, F. Matsukura, and H. Ohno, Appl. Phys. Lett. **90**, 212507 (2007).
[11] S. Ikeda, J. Hayakawa, Y. Ashizawa, Y. M. Lee, K. Miura, H. Hasegawa, M. Tsunoda, F. Matsukura, and H. Ohno, Appl. Phys. Lett. **93**, 082508 (2008).
[12] X.-G. Zhang, W. H. Butler, and A. Bandyopadhyay, Phys. Rev. B **68**, 092402 (2003).
[13] F. Bonell, S. Andrieu, A. M. Bataille, C. Tiusan, and G. Lengaigne, Phys. Rev. B **79**, 224405 (2009).
[14] F. Bonell, S. Andrieu, F. Bertran, P. Lefèvre, A. Taleb Ibrahimi, E. Snoeck, C.-V. Tiusan, and F. Montaigne, IEEE Trans. Magn. **45**, 3467 (2009).
[15] Y. Ando, T. Miyakoshi, M. Oogane, T. Miyazaki, H. Kubota, K. Ando, and S. Yuasa, Appl. Phys. Lett. **87**, 142502 (2005).
[16] S. G. Wang, G. Han, G. H. Yu, Y. Jiang, C. Wang, A. Kohn, and R. C. C. Ward, J. Magn. Magn. Mater. **310**, 1935 (2007).
[17] H. L. Meyerheim, R. Popescu, J. Kirschner, N. Jedrecy, M. Sauvage-Simkin, B. Heinrich, and R. Pinchaux, Phys. Rev. Lett. **87**, 076102 (2001).
[18] V. Serin, S. Andrieu, R. Serra, F. Bonell, C. Tiusan, L. Calmels, M. Varela, S. J. Pennycook, E. Snoeck, M. Walls, and C. Colliex, Phys. Rev. B **79**, 144413 (2009).
[19] G. X. Du, S. G. Wang, Q. L. Ma, Y. Wang, R. C. C. Ward, X.-G. Zhang, C. Wang, A. Kohn, and X. F. Han, Phys. Rev. B **81**, 064438 (2010).
[20] T. Urano and T. Kanaji, J. Phys. Soc. Jpn. **57**, 3403 (1988).
[21] K. Watanabe, T. Yamazaki, I. Hashimoto, and M. Shiojiri, Phys. Rev. B **64**, 115432 (2001).
[22] J. Mathon and A. Umerski, Phys. Rev. B **74**, 140404 (2006).
[23] P. Bose, A. Ernst, I. Mertig, and J. Henk, Phys. Rev. B **78**, 092403 (2008).
[24] H. L. Meyerheim, R. Popescu, N. Jedrecy, M. Vedpathak, M. Sauvage-Simkin, R. Pinchaux, B. Heinrich, and J. Kirschner, Phys. Rev. B **65**, 144433 (2002).
[25] K. Miyokawa, S. Saito, T. Katayama, T. Saito, T. Kamino, K. Hanashima, Y. Suzuki, K. Mamiya, T. Koide, and S. Yuasa, Jpn. J. Appl. Phys., Part 2 **44**, L9 (2005).
[26] S. G. Wang, A. Kohn, C. Wang, A. K. Petford-Long, S. Lee, R. Fan, J. P. Goff, L. J. Singh, Z. H. Barber, and R. C. C. Ward, J. Phys. D **42**, 225001 (2009).
[27] Q. L. Ma, S. G. Wang, J. Zhang, Y. Wang, R. C. C. Ward, C. Wang, A. Kohn, X.-G. Zhang, and X. F. Han, Appl. Phys. Lett. **95**, 052506 (2009).
[28] S. Lozano-Perez, V. de Castro Bernal, and R. J. Nicholls, Ultramicroscopy **109**, 1217 (2009).
[29] J. L. Hutchison, J. M. Titchmarsh, D. J. H. Cockayne, R. C. Doole, C. J. D. Hetherington, A. I. Kirkland, and H. Sawada, Ultramicroscopy **103**, 7 (2005).
[30] L. Y. Chang, A. I. Kirkland, and J. M. Titchmarsh, Ultramicroscopy **106**, 301 (2006).
[31] C. Wang, S. G. Wang, A. Kohn, R. C. C. Ward, and A. K. Petford-Long, IEEE Trans. Magn. **43**, 2779 (2007).
[32] P. Goodhew and A. Bleloch, Mater. World **11**, 23 (2003).
[33] O. L. Krivanek, N. Delby, and A. R. Lupini, Ultramicroscopy **78**, 1 (1999).
[34] R. F. Egerton, *Electron Energy-Loss Spectroscopy in the Electron Microscope*, 2nd ed. (Plenum Press, New York, London, 1996).
[35] N. Bonnet, N. Brun, and C. Colliex, Ultramicroscopy **77**, 97 (1999).
[36] P. Trebbia and N. Bonnet, Ultramicroscopy **34**, 165 (1990).
[37] B. D. Yu and J.-S. Kim, Phys. Rev. B **73**, 125408 (2006).
[38] M. Sicot, S. Andrieu, F. Bertran, and F. Fortuna, Phys. Rev. B **72**, 144414 (2005).
[39] H. Oh, S. B. Lee, J. Seo, H. G. Min, and J.-S. Kim, Appl. Phys. Lett. **82**, 361 (2003).
[40] C. L. Jia, M. Lentzen, and K. Urban, Science **299**, 870 (2003).
[41] K. Yoshida, T. Kawai, T. Nambara, S. Tanemura, K. Saitoh, and N. Tanaka, Nanotechnology **17**, 3944 (2006).

[42] C. Wang, Ph.D. thesis, University of Oxford, 2008.
[43] A. I. Kirkland and R. R. Meyer, Microsc. Microanal. **10**, 401 (2004).
[44] J. L. Vassent, M. Dynna, and A. Marty, J. Appl. Phys. **80**, 5727 (1996).
[45] S. J. Pennycook, D. E. Jesson, A. J. McGibbon, and P. D. Nellist, J. Electron Microsc. **45**, 36 (1996).
[46] S. J. B. Reed, Ultramicroscopy **7**, 405 (1982).
[47] R. F. Egerton, Ultramicroscopy **107**, 575 (2007).
[48] C. R. Seabourne, A. J. Scott, G. Vaughan, R. Brydson, S. G. Wang, R. C. C. Ward, C. Wang, A. Kohn, B. Mendis, and A. K. Petford-Long, Ultramicroscopy (to be published).
[49] B. M. Lairson, A. P. Payne, S. Brennan, N. M. Rensing, B. J. Daniels, and B. M. Clemens, J. Appl. Phys. **78**, 4449 (1995).
[50] P. W. Tasker and D. M. Duffy, Surf. Sci. **137**, 91 (1984).
[51] L. Z. Mezey and J. Giber, Jpn. J. Appl. Phys., Part 1 **21**, 1569 (1982).
[52] L. Vitos, A. V. Ruban, H. L. Skriver, and J. Kollár, Surf. Sci. **411**, 186 (1998); H. Chamati, N. I. Papanicolaou, Y. Mishin, and D. A. Papaconstantopoulos, *ibid.* **600**, 1793 (2006); J. Yu, X. Lin, J. Wang, J. Chen, and W. Huang, Appl. Surf. Sci. **255**, 9032 (2009).
[53] J. P. Velev, K. D. Belashchenko, S. S. Jaswal, and E. Y. Tsymbal, Appl. Phys. Lett. **90**, 072502 (2007).